Ann Nucl Med (2016) 30:225–233
DOI 10.1007/s12149-015-1050-y

ORIGINAL ARTICLE

Comparison of integrated whole-body PET/MR and PET/CT: Is PET/MR alternative to PET/CT in routine clinical oncology?

Shirou Ishii[1] · Daisuke Shimao[2] · Takamitsu Hara[3] · Masayuki Miyajima[1] · Ken Kikuchi[1] · Masashi Takawa[4] · Kensuke Kumamoto[4] · Hiroshi Ito[3] · Fumio Shishido[1]

Received: 30 July 2015 / Accepted: 1 December 2015 / Published online: 16 December 2015

Abstract
Purpose To compare the diagnostic accuracy of whole-body PET/CT and integrated PET/MR in relation to the total scan time durations.
Methods One hundred and twenty-three (123) patients (40 males and 83 females; mean age 59.6 years; range 20–83 years) with confirmed primary cancer and clinical suspicion of metastatic disease underwent whole-body 18F-FDG-PET/CT and 18F-FDG-PET/MR. Data acquisition was done after intravenous administration of 110–301 MBq radioactivity of 18F-FDG, and PET/MR data were acquired after the PET/CT data acquisition. The mean uptake times for PET/CT and PET/MR acquisition were 68.0 ± 8.0 and 98.0 ± 14 min, respectively. Total scan time was 20.0 and 25.0 min for whole-body PET/CT and PET/MR imaging.
Results The reconstructed PET/CT and PET/MR data detected 333/355 (93.8 %) common lesions in 111/123 (90.2 %) patients. PET/CT and PET/MR alone detected 348/355 and 340/355 lesions, respectively. No significant ($p = 0.08$) difference was observed for the overall detection efficiency between the two techniques. On the other hand, a significant difference was observed between the two techniques for the detection of lung ($p = 0.003$) and cerebrospinal ($p = 0.007$) lesions. The 15 lesions identified by PET/CT only included 8 lung, 3 lymph nodes, 2 bone, and 1 each of peritoneal and adrenal gland lesions. On the other hand, 7 (6 brain metastatic lesions and 1 bone lesion) were identified by PET/MR only.
Conclusion Integrated PET/MR is a feasible whole-body imaging modality and may score better than PET/CT for the detection of brain metastases. To further prove diagnostic utility, this technique requires further clinical validation.

Keywords PET/MR · PET/CT · Whole-body · Oncology · Lesion detectability

Introduction

A recent introduction of the integrated PET/MR system into clinical practice is viewed as having significant advantages over the existing PET/CT hybrid imaging. PET/MR combination provides higher image contrast as well as spatial and temporal correlation for PET and MR data being acquired simultaneously. Additionally, MRI in hybrid PET/MR imaging provides useful information about the pathophysiological processes [1]. Moreover, PET/MR may reduce the radiation exposure in patients as compared to the currently used PET/CT combination which may be of special significance in pediatric patients.

In oncology, PET/MR is potentially more useful than PET/CT in evaluating a single body region or a particular component, due to the superior soft tissue contrast afforded by MRI over CT, and such contrast is crucial for delineating

✉ Shirou Ishii
shirou@fmu.ac.jp

[1] Department of Radiology, Fukushima Medical University Hospital, 1, Hikarigaoka, Fukushima, Fukushima Prefecture, Japan

[2] Department of Radiological Technology, Faculty of Health Sciences, Hokkaido University of Science, Sapporo, Hokkaido, Japan

[3] Advanced Clinical Research Center, Fukushima Medical University, Fukushima, Japan

[4] Department of Organ Regulatory Surgery, Fukushima Medical University, Fukushima, Japan

tumor location and the extent of invasion. Furthermore, the feasibility and utility of PET/MR for head and neck cancer, prostate cancer, and bone lesions, among others, have been highlighted in several recent reports [1–9].

Despite the promising findings of PET/MR, the clinical validation of the use of this imaging modality for whole-body examination has not been investigated so far. The latter is attributed mainly due to the inherent problem of MR in detecting smaller lung lesions and the longer acquisition time. Although few studies have reported the PET/MR use for whole-body evaluation, there has yet been a wide variability (acquisition time/workflow) in MRI acquisitions' protocols [10–13].

Therefore, in the present study, we evaluated the comparative diagnostic efficacy of whole-body PET/MR and PET/CT imaging for the accurate detection of malignant and benign lesions in cancer patients with strong suspicion of malignant disease.

Materials and methods

Patient populations

From November 2013 to July 2014, we evaluated 123 consecutive patients (40 men and 83 women; mean age 59.6 years, range 20–83 years). All patients underwent single-injection dual-imaging with 2-[fluorine-18]-fluoro-2-deoxy-D-glucose (FDG)-PET/CT followed by PET/MR for the staging and following up of malignant lesions.

The inclusion criteria were as follows: (a) patients who had had or were highly suspected of having malignant lesions; (b) those aged older than 20 years; (c) those who were without pregnancy; (d) those with an ability to tolerate long durations of image acquisition; and (d) those with no contraindications for MR examination, such as pacemakers and metal implants. All patients who had met these criteria and agreed to undergo PET/MR were included. One patient who underwent PET/CT and PET/MR was excluded from this study because of degraded image quality due to a high blood sugar level.

Patients with the following malignancies were included: breast carcinoma, $n = 33$ (30 invasive ductal carcinoma and 3 noninvasive ductal carcinoma); lung carcinoma, $n = 21$ (14 adenocarcinoma, five squamous carcinoma, one small cell carcinoma, and one metastasis); lymphoma, $n = 14$ (six diffuse large B cell lymphoma, six follicular lymphoma, one angioimmunoblastic T cell lymphoma, and one nodular sclerosis Hodgkin lymphoma); colorectal carcinoma, $n = 10$; ovarian carcinoma, $n =$ seven; uterus carcinoma, $n =$ six; pancreas carcinoma, $n =$ five; esophageal carcinoma, $n =$ five; thyroid carcinoma, $n =$ three; hepatocellular carcinoma, $n =$ two; stomach carcinoma, $n =$ two; multiple myeloma, $n =$ two; cancer of unknown origin, $n =$ two; and other tumors, $n = 11$.

PET/MR and PET/CT protocols

Imaging protocols

All patients fasted for at least 4 h or skipped one meal before their examination. The mean glucose level at the time of injection was 100 ± 12 mg/dl (range 79–164). Patients were injected with 110–301 MBq of FDG. Although PET/CT preceded PET/MR in almost all examinations, PET/MR examinations were performed before PET/CT in two cases because of room availability. After the FDG injection, PET/CT was started at a mean of 63 ± 8 min, and PET/MR at a mean of 98 ± 14 min. Following the PET/CT examination, patients were immediately moved to the PET/MR room which was located next door to minimize the time gap between the imaging procedures. No contrast agent was used in any of the patients for either PET/CT or PET/MR.

PET/CT

FDG-PET/CT data were acquired on a Biograph mCT with 128-slice CT (Siemens Healthcare, Erlangen, Germany). Acquisition parameters for CT were as follows: tube voltage of 120 kVp; auto mAs (reference tube current of 80 mAs); a rotation time of 0.5 s; a matrix of 512×512; and reconstruction with a 3 mm slice thickness and a 2-mm increment. CT data were acquired during expiratory breath holding.

Acquisition of PET data started from the upper thigh and finished at the head during shallow breathing. The acquisition time was 2–3 min per bed position (BP), with 6–8 BPs (each 21.8 cm). A matrix of 200×200 was used. The PET data were reconstructed using ordered subset expectation maximization (3D-OSEM) containing three iterations and 21 subsets, with time of flight (TOF), point spread function (PSF), and a Gaussian filter of 3 mm in full width at half maximum. Attenuation correction was performed based on the data obtained from the CT scan acquired prior to the PET scan.

PET/MR

PET/MR data were obtained using an integrated whole-body PET/MR system (Biograph mMR; Siemens Healthcare) with a 3.0-tesla MRI scanner. The technical performance of the Biograph mMR and Biograph mCT was summarized in a recent paper [14].

Acquisition of the PET data began at the upper thigh and finished at the head, with shallow breathing during MRI acquisition. The PET data acquisition time was 3 min per BP, with 4–6 BPs (each 25.8 cm). Besides the Dixon

sequence for attenuation correction, axial half-Fourier acquisition single-shot turbo spin-echo (HASTE) and coronal turbo spin-echo T1-weighted (TSE-T1W) images (both with a 6 mm slice thickness) were obtained. The data of the chest and upper abdominal regions of TSE-T1WI were acquired with breath holding, and the data of other regions of TSE-T1WI and HASTE were obtained with shallow breathing. The parameters of HASTE were as follows: repetition time, 750 ms; echo time, 73 ms; flip angle, 120°; matrix, 384 × 276; slice thickness, 6 mm; slice gap, 1.8 mm. The parameters of TSE-T1W images were as follows: repetition time, 500 ms; echo time, 8.2 ms; flip angle, 140°; matrix, 384 × 931; slice thickness, 6 mm; slice gap, 1.8 mm. A matrix of 172 × 172 was used for PET in PET/MRI. The PET data were reconstructed using 3D-OSEM containing three iterations and 21 subsets and a Gaussian filter of 5 mm in full width at half maximum. The PET data underwent automatic attenuation correction with attenuation maps generated from the two-point Dixon sequence.

Total examination room time for the PET/MR examination (the period between the patient entering and leaving the room) was about 25 min and included headphone and coil placement, planning, and acquisition. The corresponding room time for PET/CT examination was approximately 20 min.

Table 1 shows the technical differences between the PET/CT and PET/MR examinations.

Image evaluation

An axial HASTE of 6 mm thickness, TSE-T1W coronal images of 6 mm thickness, and attenuation-corrected PET images were used for PET/MR evaluation. Two-point Dixon imaging was used for attenuation correction only. CT images of a 3 mm slice thickness and a 2-mm increment with volume data- and attenuation-corrected PET images were used for PET/CT evaluation. Readers fused the PET and CT or MR images and could change the windows, as well as measure the length or density/intensity of the lesions on the image viewer. Image analysis was performed using a commercial software package (EV Insite, PSP Corp., Tokyo, Japan).

PET/CT and PET/MR images were evaluated by two readers, and detection by each modality was defined as follows:

(a) PET/CT: detected by both PET and CT, only PET, or only CT
(b) PET/MR: detected by both PET and MR, only PET, or only MR

Two readers, a board-certified radiologist with 11-year experience (Reader 1) and a board-certified nuclear medicine physician with 9-year experience (Reader 2), were aware of primary malignancy, but were blinded to clinical history and clinical findings such as prior images or laboratory data. The readers recorded the number and locations of the malignant lesions and also checked benign lesions, excluding simple cysts, that potentially required treatment, further investigation, or follow-up. As described in previous study, in cases with excessive numbers of PET-positive lesions, up to five lesions per organ or compartment were chosen to avoid bias from individual patients [10]. To avoid evaluating PET/CT and PET/MR of a patient by the same reader, Reader 1 read the data of patients 1–62 of PET/MR and 63–123 of PET/CT, and Reader 2 read the data of patients 1–62 of PET/CT and 63–123 of PET/MR.

Table 1 Technical differences between PET/CT and PET/MR examinations

	PET/CT	PET/MR
Modality	Biograph mCT	Biograph mMR
Sequences used for image analysis	Axial CT images with 3 mm slice thickness reconstruction and 2-mm increment (volume data)	HASTE axial 6 mm (gap 30 %) TSE-T1WI coronal 6 mm (gap 30 %)
Matrix of PET	200 × 200	172 × 172
Matrix of CT or MRI	512 × 512	HASTE: 384 × 276 TSE-T1W: 384 × 931
FOV (mm)	500 × 500	HASTE: 450 × 323 TSE-T1W: 450 × 1091
Acquisition time of PET	2–3 min per bed position	3 min per bed position
Acquisition time of CT or MRI	10 s for whole body	HASTE: 26 s per bed TSE-T1W: 52 s per bed
Total examination time	About 20 min	About 25 min
Scan start time after injection	63 ± 8 min	98 ± 14 min
Reconstruction of PET image	OSEM + TOF + PSF	OSEM

Finally, the imaging findings of the two modalities were compared by a third reader, a board-certified radiologist and nuclear medicine physician with 15-year experience in general radiology (Reader 3), who was aware of all patient data, including prior or current imaging findings, clinical data, and surgical and pathological records.

Statistical analysis

Concordance rate between PET/CT and PET/MR was calculated as a percentage. To test the differences in detection rate between PET/CT and PET/MR, Chi-square test was used. A p value below 0.05 was considered statistically significant. Statistical analysis was performed using Microsoft Excel 2013 for Windows.

Results

Of the 123 patients, 60 had malignant lesions, and among those patients, PET/MR and PET/CT detected lesions in 58 and 59 patients, respectively. In one patient with multiple myeloma, no lesions were detected by PET/CT (Fig. 1). Similarly, PET/MR could not detect

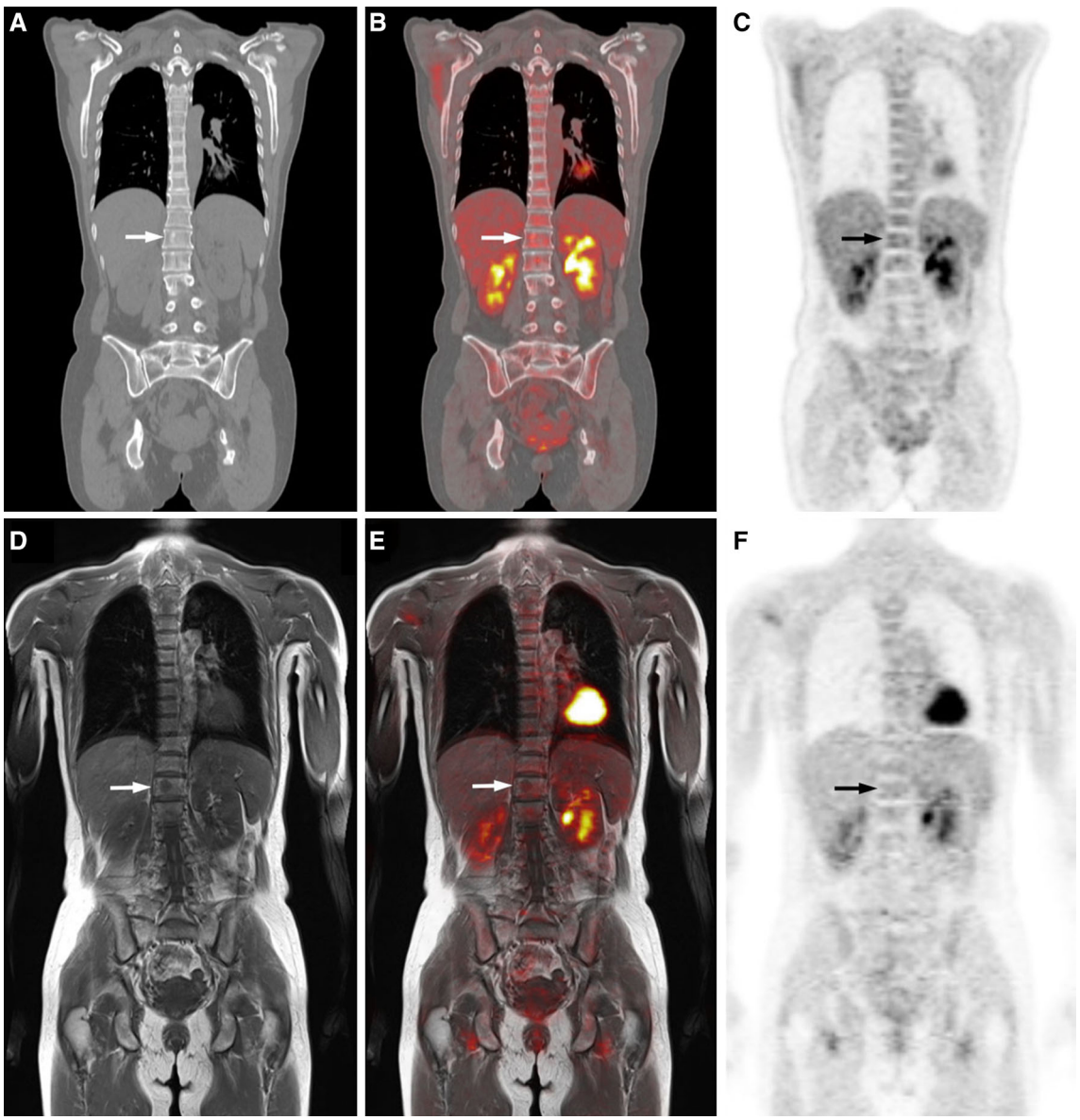

Fig. 1 A 42-year-old female with multiple myeloma. No significant bone lesions were visible on coronal CT image (**a**), fused PET/CT images (**b**), both 18F-FDG-PET images acquired on PET/CT (**c**), or PET/MR (**f**). Only T1W coronal image (**d**) showed a round, low-intensity lesion in the L1 vertebra consistent with myeloma (*arrow*). The co-registered 18F-FDG-PET and T1WI image (**e**) also shows no significant uptake in the L1 vertebral lesion

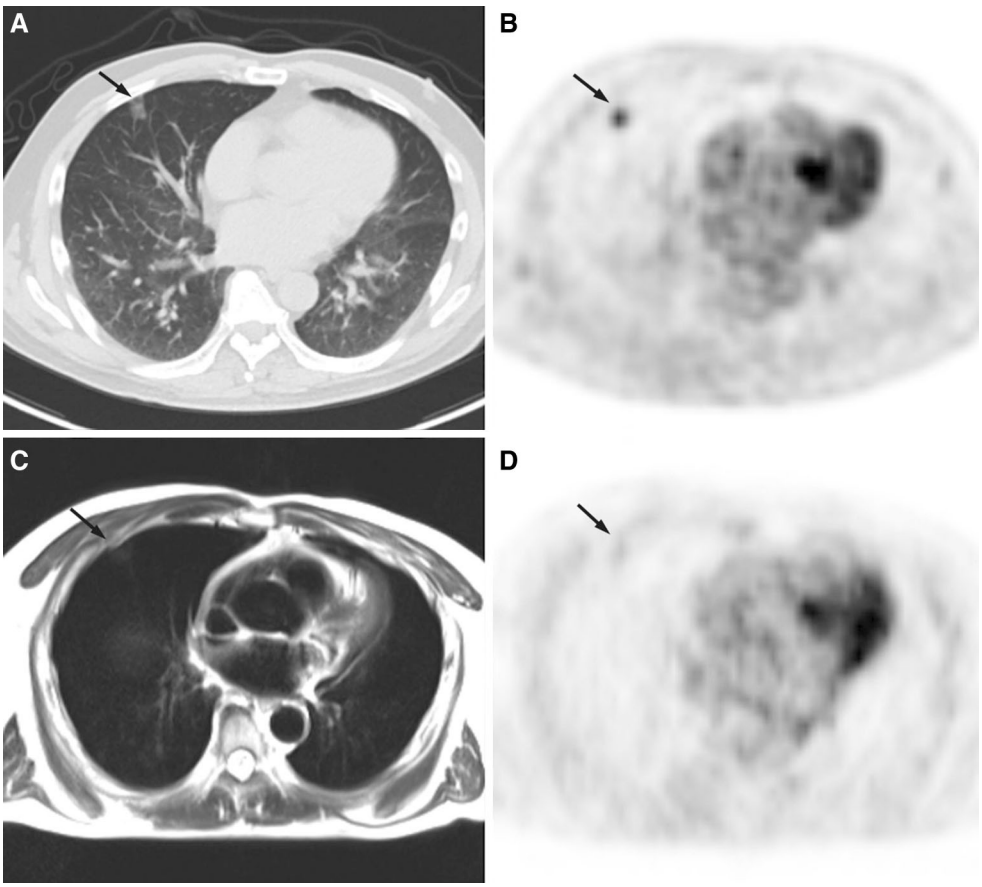

Fig. 2 A 66-year-old man with lung adenocarcinoma. Axial CT image (**a**) and PET of PET/CT (**b**) show FDG-avid ground glass opacity in the right middle lobe (*arrow*). Although PET derived from PET/MR (**d**) indicates at least a weak uptake of the right middle lobe, identification of the lung nodule is difficult in the HASTE image only (**c**) (*arrow*)

Table 2 Malignant lesions detected by PET/CT and PET/MR

	PET/CT	PET/MRI	*p* value
No. of lesion-positive patients (60 of 123)	59	58	0.55
Total no. of detected lesions (out of 355)	348 (271, 63, 14)	340 (225, 95, 20)	0.08
Lymph node	175 (144, 28, 3)	172 (122, 48, 2)	0.08
Lung	76 (66, 3, 7)	68 (42, 19, 7)	0.003
Bone	35 (19, 16, 0)	34 (20, 13, 1)	0.55
Cerebrospinal	12 (3, 5, 4)	18 (3, 5, 10)	0.007
Peritoneum	15 (13, 2, 0)	14 (11, 3, 0)	0.30
Adrenal	5 (4, 1, 0)	4 (3, 1, 0)	0.29
Other regions	30 (22, 8, 0)	30 (24, 6, 0)	

Values given in parentheses indicate the detected number by both PET and CT (or MR), only PET, and only CT (or MRI), respectively

lesions in one patient with breast cancer and one with lung cancer (Fig. 2).

A total of 355 malignant lesions were identified, consisting of 175 in lymph nodes, 76 in the lungs or pleura, 36 in the bones, 18 in the brain and spinal cord, 15 in the peritoneum, 12 in muscle or soft tissue, eight in mammary glands, five in adrenal glands, three in the esophagus, two in the mediastinum, two in the pancreas, and one each in the bile duct, liver, and salivary gland. Out of the 355 lesions, 348 were detected by PET/CT and 340 by PET/MR. There were no significant differences in the detection rates for malignant lesions between PET/CT and PET/MR ($p = 0.08$). However, significant differences were observed for lung lesion ($p = 0.003$) and cerebrospinal lesions ($p = 0.007$) (Table 2).

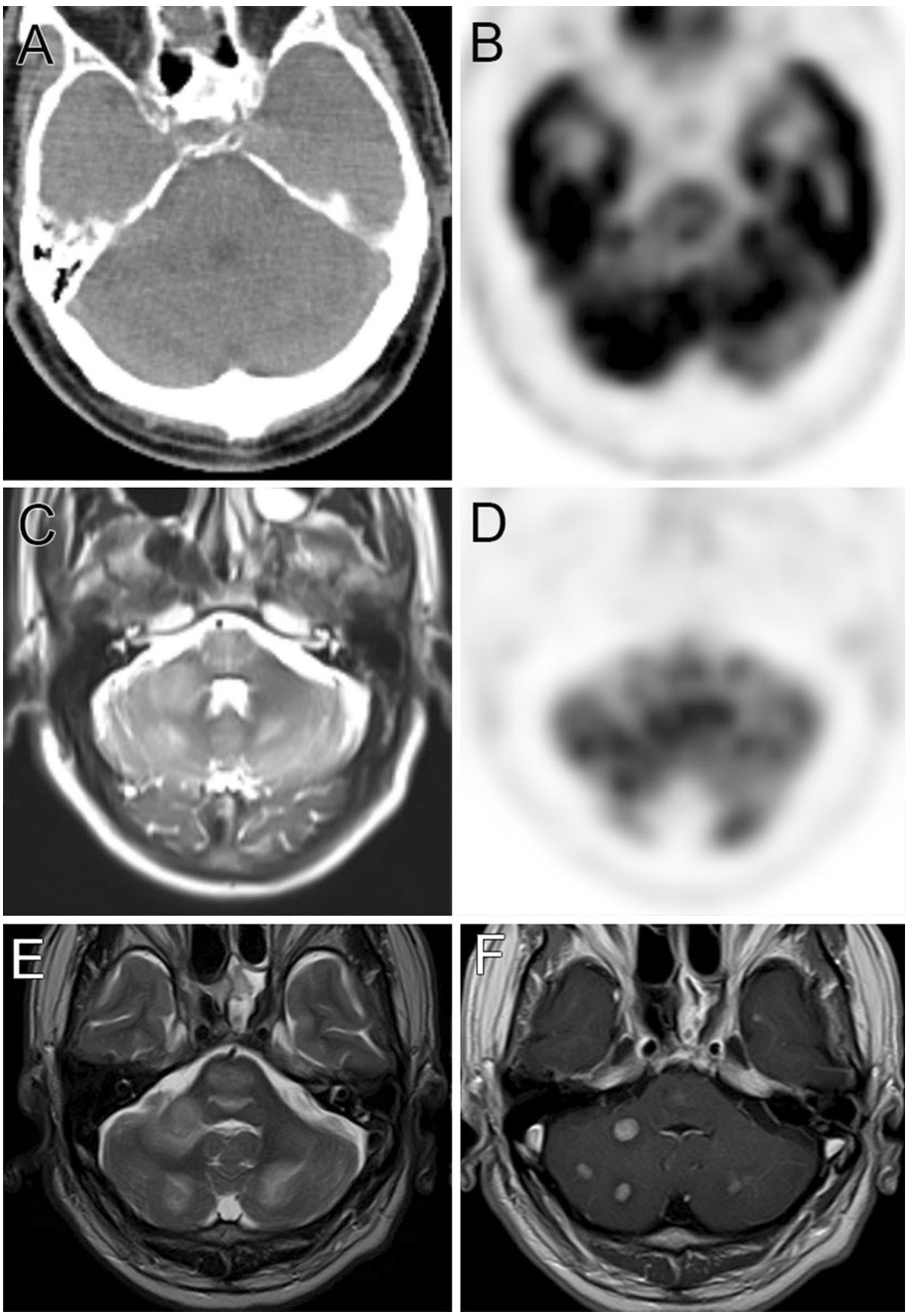

Fig. 3 A 62-year-old man with multiple brain metastases from lung cancer. Detection of brain lesions with CT (**a**), PET of PET/CT (**b**), and PET of PET/MR (**d**) is difficult. In contrast, the HASTE image (**c**) shows multiple high-intensity lesions in the cerebellum and pons, consistent with brain metastases with parenchymal edema. Brain MRI performed 2 days later clearly shows multiple high-intensity foci on T2WI (**e**) and multiple lesions on gadolinium-enhanced T1WI imaging (**f**)

In 111 patients (90.2 %), both PET/MR and PET/CT showed 333 foci out of 355 lesions, with an agreement rate of 93.8 %.

PET/CT revealed 15 lesions (4.2 %) that were not identified by PET/MR in nine patients (7.3 %), while PET/MR revealed seven lesions (2.0 %) in three patients (2.4 %) that were not identified by PET/CT. The 15 foci identified only by PET/CT comprised eight lung lesions, three lymph node lesions, two bone lesions, one peritoneal lesion, and one adrenal gland lesion. The seven foci detected only by PET/MR comprised six brain metastases and one bone lesion (Figs. 1, 2, 3; Table 2). Benign lesions detected by either PET/CT or PET/MR are shown in Table 3.

Discussion

Our study showed that PET/MR and PET/CT were comparable in a whole-body oncologic evaluation. As expected, some brain metastases and bone lesions were detected by PET/MR only, whereas PET/CT identified more lesions overall, mostly in the lungs. Several recent studies

Table 3 Details of benign lesions detected only by each modality

	PET/CT	PET/MRI
Detected lesions	Fatty liver: 4	Brain infarction: 6
	Gall stone: 4	Brain hemorrhage: 3
	Lung nodule: 3	Bone lesion: 3
	Pulmonary emphysema: 3	Gall stone: 3
	Intestinal pneumonia: 2	Thyroid nodule: 1
	Renal stone: 2	Endometriosis: 1
	Adrenal adenoma: 1	Endometrial polyp: 1
	Bronchopneumonia: 1	
	Renal angiomyolipoma: 1	

compared the detectability of whole-body integrated PET/MR and PET/CT using FDG or other probes and also found comparable results with an agreement rate of 97.4–98.7 % in 32–80 patients with a variety of malignant lesions [10–12]. The agreement rates of these studies were a little higher than our result of 93.8 %; however, the methods used in the previous studies differed from ours regarding the MRI protocols, study time, acquisition time of PET, and scan start time after injection. Evidence of whether PET/MR could be a comparable alternative or superior to PET/CT was limited in the previously reported studies. For instance, there was a time lapse of 54–99 min on average after PET/CT and before PET/MR, and the acquisition time of PET in PET/MR was longer than in PET/CT by 3–10 min per BP in other studies. Moreover, another study used the 3D Dixon sequence only, while others used Dixon, T1WI, T2WI, and DWI sequences; thus, the acquisition time varied from less than 20 to 60 min. The more the sequences that were used, the more the lesions that could be detected, whereas in the present study, we used axial HASTE and coronal TSE-T1W images of 6 mm thickness as the standard protocol, considering the total examination time to be approximately 25 min. Moreover, we started PET/MR acquisition soon after the PET/CT acquisition with a delay of about 36 min. When more protocols such as thin slice, 3D image, DWI, functional MRI, and MRS are used, the time for MRI takes 60 or even 90 min. In such a circumstance, it is not practical to perform PET/MR for a routine whole-body examination, considering the burden on the patient, examination schedule, and workflow. The clinical protocol for PET/CT with a multi-detector CT is relatively simple and mainly fixed, whereas scan protocols for MRI are more complex and require attention to slice thickness, slice direction, and imaging protocols in order to complete the acquisition within the restricted time of PET/MR. In the present study, we limited the scan sequence and used a relatively thick slice to complete the scanning within the time provided. In terms of an appropriate routine protocol for PET/MR, further studies are needed for whole-body and per-lesion or per-organ evaluations.

Although no significant difference in overall detectability was found between the two modalities, PET/CT detected more lesions than PET/MR in our protocol. This is mainly due to the lower detectability of small lung lesions with MRI, large slice thickness of MRI, and differences in performance of the PET scanners. Notably, although the counting of all lesions including small ones may not be important for the patient's clinical management, we experienced a case of small ground glass opacity (GGO) in lung adenocarcinoma that was not detected by PET/MR (Fig. 2). Recent reports described no significant difference regarding detection rate of FDG-avid lung nodules between PET/CT and PET/MR using dedicated lung protocols of 3D dual-echo gradient-echo sequence or contrast-enhanced volumetric interpolated breath-hold examination sequences (VIBE); however, the detection rate of small lung lesions by PET/MR was reported to be lower [15, 16]. Indeed, significant differences were found in the detection rates of lung nodules between PET/CT and PET/MR in this study. In another report, the sensitivity of PET/MR was 70.3 % for all lung nodules, and 22.9 % for non-FDG-avid nodules [17]. Thin-slice images can be used to evaluate lesions with a multi-planar PET/CT; however, it is not easy to acquire thin slices or 3D images of whole-body routinely by MRI due to its long acquisition time. In addition, MRI has difficulty in detecting not only small lung nodules or GGO, but also lung parenchymal changes such as emphysema. As for cases where PET/MR is performed for whole-body evaluation, additional chest CT is recommended for screening lung nodules, especially in cases of lung metastases with weak FDG uptake such as adenocarcinoma or thyroid differentiated carcinoma. More dedicated and appropriate MR protocols for imaging the lungs are expected in future, especially for depicting pulmonary diseases.

Eiber et al. reported that PET/MR, including the TSE-T1W sequence, was superior to PET/CT for anatomic delineation, which was consistent with the correct classification of malignant bone lesions in their study of 33 patients with 98 bone lesions [3]. It is possible that bone lesions with weak uptake of FDG such as bone metastases from thyroid cancer or hepatocellular carcinoma and multiple myeloma, as in our case (Fig. 1), are more likely to be detected by PET/MR than PET/CT.

With regard to benign lesions, the readers could identify more lesions such as fatty liver lesions, small calcified lesions, and lung lesions by PET/CT compared to PET/MR. In contrast, brain, bone, and utero-ovarian lesions were identified by PET/MR (Table 2). This difference can be explained by the advantages of CT with its thin-slice image

acquisition, calcification depiction, and lung lesion evaluation, in comparison with the superior soft tissue contrast of MRI.

In this study, we only focused on whole-body lesion detectability by PET/MR in short examination time. However, PET/MR has the potential to be more useful for evaluating local lesions to assess invasion range, and for analyzing tissue characterization of the tumor than whole-body screening, considering the advantages of MRI. Although the average examination using PET/MR takes 66 min, it leads to better clinical management than PET/CT, as reported by Catalano et al. [13]. Furthermore, Al-Nabnahi et al. reported a 10 % improvement in local staging with PET/MR compared to PET/CT, suggesting that using PET/MR for major lesion evaluation, following whole-body screening by PET/CT could be more effective [12].

There are several limitations in our study.

The number of female patients was almost twice that of males in the present study, introducing the possibility of bias. The main reason is that there were many patients with female-specific cancers such as breast or utero-ovarian cancers.

Although Biograph mCT and Biograph mMR showed equivalent performance, the technological difference between PET/MR and PET/CT scanners may have affected the detection of small lesions. In addition, only 3D-OSEM was used for PET/MR reconstruction, whereas the reconstruction of PET/CT was performed with 3D-OSEM using TOF and PSF, which have been reported to improve contrast and signal-to-noise ratio [18, 19]. In our lung cancer case with GGO that was undetected by PET/MR, the maximum standard uptake value (SUV) of the lesion on PET/CT was 4.2, which was significantly higher than the 1.1 achieved by PET/MR (Fig. 2). However, even without TOF + PSF, the SUV max of the GGO in PET/CT was 3.2. MRI-based attenuation correction is currently an underestimation, with the SUV of lesions reported as higher in PET/CT than in PET/MR, probably because of the different attenuation corrections used. Therefore, MRI-based AC without bone segmentation affects detection of small lesions as well as those in bone or near bone. Also, various factors such as difference in matrix size, Gaussian filter, and others might affect lesion detection. Indeed, there were some cases where two adjacent PET-positive lymph nodes were clearly discriminated in PET of PET/CT, but were difficult to discriminate and were therefore judged as one lymph node in the PET of PET/MR in this study. These differences affected SUV and lesion detectability in the present study. In our institution, PET/CT and PET/MR were introduced at around the same time, and the latest PET technology for PET/CT has been advantageous for comparison with PET/MR.

Although we started the PET/MR acquisition soon after the PET/CT acquisition, there was a difference of about 35 min between the start times of PET/CT and PET/MR, and the delayed PET acquisition could have improved lesion detection [20, 21].

Histopathological findings were not feasible in most of the metastatic lesions, and they were diagnosed on the basis of imaging findings including follow-up study and clinical data.

No contrast medium was given for either examinations, and a dedicated lung sequence was not used in the PET/MR examinations. Had such sequence been used, it may have yielded different results.

Conclusion

This study showed that integrated PET/MR is a clinically feasible whole-body imaging modality for routine oncologic examination. However, due to the thick slices of MRI, PET/MR has difficulties in detecting not only non-FDG-avid lung nodules, but also small lesions such as those in lymph nodes. The use of PET/MR for whole-body evaluation without chest CT has not yet been validated. To improve small lesion detection, the following may be effective: thin-slice images; 3D VIBE of the lung lesion or abdominal lesions that could be performed in a relatively short time; or adding diffusion-weighted images of abdominal lesions. Further studies are required for optimal MRI sequence for lesion detection in whole-body imaging. At present, PET/CT cannot be completely replaced by PET/MR. Gadolinium-enhanced brain MRI is also often added to whole-body PET/CT scans. Both CT and MRI play a complementary role in the current setting, and further studies are needed to establish scan protocols for high-speed acquisition of whole-body images and acquisition methods for better lung evaluation in routine clinical settings.

Acknowledgments We are grateful for the assistance of Seiichi Takenoshita, doctors of the Department of Organ Regulatory Surgery and Radiology, and the staff of Advanced Clinical Research Center for their support in performing this study.

Compliance with ethical standards

Conflict of interest The authors declare that there is no conflict of interest.

References

1. Czernin J, Herrmann K. The potential of PET/MRI imaging in oncology: a comment to a summary report of the first PET/MRI workshop in Tuebingen in 2012. Mol Imaging Biol. 2013;15:372–3.

2. Czernin J, Ta L, Herrmann K. Does PET/MR imaging improve cancer assessments? Literature evidence from more than 900 patients. J Nucl Med. 2014;55(Supplement 2):59S–62S.
3. Eiber M, Takei T, Souvatzoglou M, Mayerhoefer ME, Fürst S, Gaertner FC, et al. Performance of whole-body integrated 18F-FDG PET/MR in comparison to PET/CT for evaluation of malignant bone lesions. J Nucl Med. 2014;55:191–7.
4. Huellner MW, Appenzeller P, Kuhn FP, Husmann L, Pietsch CM, Burger IA, et al. Whole-body nonenhanced PET/MR versus PET/CT in the staging and restaging of cancers: preliminary observations. Radiology. 2014;273:859–69.
5. Afshar-Oromieh A, Haberkorn U, Schlemmer HP, Fenchel M, Eder M, Eisenhut M, et al. Comparison of PET/CT and PET/MRI hybrid systems using a 68 Ga-labelled PSMA ligand for the diagnosis of recurrent prostate cancer: initial experience. Eur J Nucl Med Mol Imaging. 2014;41:887–97.
6. Souvatzoglou M, Eiber M, Takei T, Fürst S, Maurer T, Gaertner F, et al. Comparison of integrated whole-body [11C]choline PET/MR with PET/CT in patients with prostate cancer. Eur J Nucl Med Mol Imaging. 2013;40:1486–99.
7. Partovi S, Kohan A, Vercher-Conejero JL, Rubbert C, Margevicius S, Schluchter MD, et al. Qualitative and quantitative performance of ^{18}F-FDG-PET/MRI versus ^{18}F-FDG-PET/CT in patients with head and neck cancer. AJNR Am J Neuroradiol. 2014;35:1970–5.
8. Varoquaux A, Rager O, Poncet A, Delattre BM, Ratib O, Becker CD, et al. Detection and quantification of focal uptake in head and neck tumours: (18)F-FDG PET/MR versus PET/CT. Eur J Nucl Med Mol Imaging. 2014;41:462–75.
9. Boss A, Bisdas S, Kolb A, Hofmann M, Ernemann U, Claussen CD, et al. Hybrid PET/MRI of intracranial masses: initial experiences and comparison to PET/CT. J Nucl Med. 2010;51:1198–205.
10. Drzezga A, Souvatzoglou M, Eiber M, Beer AJ, Fürst S, Martinez-Möller A, et al. First clinical experience with integrated whole-body PET/MR: comparison to PET/CT in patients with oncologic diagnoses. J Nucl Med. 2012;53:845–55.
11. Quick HH, von Gall C, Zeilinger M, Wiesmüller M, Braun H, Ziegler S, et al. Integrated whole-body PET/MR hybrid imaging: clinical experience. Invest Radiol. 2013;48:280–9.
12. Al-Nabhani KZ, Syed R, Michopoulou S, Alkalbani J, Afaq A, Panagiotidis E, et al. Qualitative and quantitative comparison of PET/CT and PET/MR imaging in clinical practice. J Nucl Med. 2014;55:88–94.
13. Catalano OA, Rosen BR, Sahani DV, Hahn PF, Guimaraes AR, Vangel MG, et al. Clinical impact of PET/MR imaging in patients with cancer undergoing same-day PET/CT: initial experience in 134 patients—a hypothesis-generating exploratory study. Radiology. 2013;269:857–69.
14. Delso G, Furst S, Jakoby B, Ladebeck R, Ganter C, Nekolla SG, et al. Performance measurements of the siemens mMR integrated whole-body PET/MR scanner. J Nucl Med. 2011;52:1914–22.
15. Rauscher I, Eiber M, Fürst S, Souvatzoglou M, Nekolla SG, Ziegler SI, et al. PET/MR imaging in the detection and characterization of pulmonary lesions: technical and diagnostic evaluation in comparison to PET/CT. J Nucl Med. 2014;55:724–9.
16. Stolzmann P, Veit-Haibach P, Chuck N, Rossi C, Frauenfelder T, Alkadhi H, et al. Detection rate, location, and size of pulmonary nodules in trimodality PET/CT-MR: comparison of low-dose CT and Dixon-based MR imaging. Invest Radiol. 2013;48:241–6.
17. Chandarana H, Heacock L, Rakheja R, DeMello LR, Bonavita J, Block TK, et al. Pulmonary nodules in patients with primary malignancy: comparison of hybrid PET/MR and PET/CT imaging. Radiology. 2013;268:874–81.
18. Akamatsu G, Ishikawa K, Mitsumoto K, Taniguchi T, Ohya N, Baba S, et al. Improvement in PET/CT image quality with a combination of point-spread function and time-of-flight in relation to reconstruction parameters. J Nucl Med. 2012;53:1716–22.
19. Prieto E, Domínguez-Prado I, García-Velloso MJ, Peñuelas I, Richter JÁ, Martí-Climent JM. Impact of time-of-flight and point-spread-function in SUV quantification for oncological PET. Clin Nucl Med. 2013;38:103–9.
20. Zhuang H, Pourdehnad M, Lambright ES, Yamamoto AJ, Lanuti M, Li P, et al. Dual time point 18F-FDG PET imaging for differentiating malignant from inflammatory processes. J Nucl Med. 2001;42:1412–7.
21. Lan XL, Zhang YX, Wu ZJ, Jia Q, Wei H, Gao ZR. The value of dual time point (18)F-FDG PET imaging for the differentiation between malignant and benign lesions. Clin Radiol. 2008;63:756–64.